Lateral Buckling of High Aspect Ratio Janus Nanowalls

Hyunsik Yoon, Abhijit Ghosh, Jung Yeon Han, Seung Hyun Sung, Won Bo Lee, and Kookheon Char**

In recent years, the fabrication of Janus materials and their potential applications has been of much interest in Materials Science. Here, we report the fabrication of an entirely novel structure–Janus nanowalls and the phenomenon of lateral buckling in them. Polymeric nanowalls were prepared with the replica molding technique and metal films, of comparable thicknesses, were then deposited on one side of the polymer nanowalls by vacuum process. During the metal deposition, the nanowalls themselves buckle laterally; this buckling is induced by the compressive residual stress in the metal film and geometric confining constraints. The feature of wrinkle patterns resulting from the lateral buckling was theoretically investigated using the scaling analysis. Theoretical results are in good agreement with the experimental observations.

1. Introduction

Inspired by the pioneering work of de Gennes and his colleagues, there has been, in recent years, much interest in fabrication and applications of Janus materials.[1–13] The term Janus was first coined by de Gennes to describe spherical particles,[1] the surface of one of whose hemispheres is chemically different from the other half, reminding one of the Roman God Janus who has two faces back to back. Fabrication of Janus nanoparticles has opened up vistas of novel applications many of which are of industrial interest. By clever tweaking of the anisotropy properties, one can use the Janus nanoparticles for a wide variety of applications such as the stabilization of emulsions, nanoscale motors, biosensors, in displays and as optical probes to name only a few.[2–13] We have also fabricated a series of Janus structures with different geometries attached to a substrate for the first time, for example, Janus nanopillars[14,15] prepared by the oblique metal deposition on vertical polymer columns placed on solid substrates. Upon metal deposition, those pillars are found to bend due to the residual stress induced by the stress relaxation of deposited layers of metal.[15]

In this paper, we report the lateral buckling in Janus nanowalls prepared by the oblique deposition of thin metal films on polymeric nanowalls standing upright on solid substrates due to the compressive residual stress of metal during deposition. While the bottoms of the walls are firmly bound to the substrate, the bilayer formed by the metal deposition is just like a freely standing vertical film. During the aluminum deposition on one side of the polymeric nanowalls, the upper part of the nanowalls is buckled due to the increase in surface area, which is so much similar to wrinkled leaves of kale.

Buckling and wrinkling phenomena in thin sheets have been regarded as classical topics in mechanics[16,17] and have thus spawned a surge of activities in recent years; examples include the differential growth driven wrinkle formation in the edges of petals of a blooming lily, the formation of periodic wrinkle patterns in an ultrathin polymer sheet floating on a fluid, and a recent piece of work proposing the shape selection rules for 3D structures attained by thin gel sheets undergoing lateral non-uniform shrinkage or with half-tone lithography technique.[18–26] Although studies on the deformation and pattern formation of soft materials under confinement have actively been pursued in recent years from both fundamental and application points of view, the freestanding bilayer system currently under investigation is quite new and novel when compared with earlier buckling studies on bilayers[27–29] including thin rigid materials deposited on thick elastomeric substrates.

We employ scaling arguments to investigate the features of wrinkling patterns induced by the lateral buckling. Our theoretical results for the dependence of wavelength and amplitude of wrinkles are in good agreement with the experimental observations.

2. Results and Discussion

The procedure to obtain buckled Janus nanowalls by the subsequent oblique metal deposition is schematically shown in

J. Y. Han, S. H. Sung, Prof. K. Char
The National Creative Research Initiative Center for Intelligent Hybrids
School of Chemical & Biological Engineering
The WCU Program of Chemical Convergence for Energy and Environment
Seoul National University
Seoul, 151-744, Korea
E-mail: khchar@plaza.snu.ac.kr
Dr. A. Ghosh, Prof. W. B. Lee
Department of Chemical and Biomolecular Engineering
Sogang University
1 Sinsu-dong, Mapo-gu, Seoul 121-732, Korea
E-mail: wblee92@sogang.ac.kr
Prof. H. Yoon
Department of Chemical Engineering
Seoul National University of Science & Technology
Seoul, 139-743, Korea

DOI: 10.1002/adfm.201200749

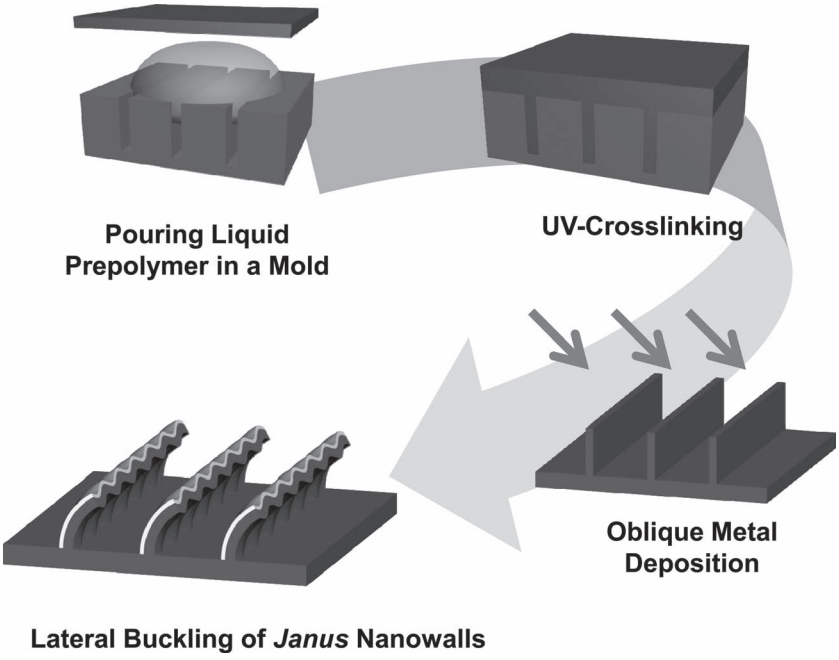

Figure 1. A schematic illustration of the fabrication of Janus nanowalls. After preparing a master mold by conventional photolithography and dry etching process, we poured a liquid-type, UV-curable prepolymer on the mold. After UV crosslinking, we detached the polymer pattern from the mold. With the help of an inclined loader, we deposited metal films on the left sides of polymeric nanowalls (i.e., Janus nanowalls). During the aluminium deposition, the Janus nanowalls spontaneously showed instabilities of lateral buckling.

Figure 1. After preparing a master produced by the conventional photolithography followed by dry etching process, a UV-curable polyurethane acrylate (PUA, 301RM, Minuta Tech) prepolymer was poured into the master.[30,31] After UV exposure to crosslink the PUA prepolymer in the master mold, the polymeric nanowalls were detached from the mold. Aluminum films (~50 nm) were then deposited obliquely only on one selected faces of the polymer nanowalls.[15] Following the above fabrication procedure, we could prepare free standing metal-polymer bilayers of nanometer film thickness standing vertically on a polymeric substrate. As previously reported,[15] aluminum metal has an inherent compressive residual stress during deposition. In other words, aluminum has a tendency to expand by reacting with polymer or oxygen on the interface. The expanding metal, being tightly attached or bound to the polymer walls, increase the surface areas of the nanowalls. Confinement at the base leads to the subsequent lateral buckling of nanowalls.

Figure 2 shows the scanning electron microscope (SEM) images of pristine polymeric nanowalls and buckled Janus nanowalls. Before the metal deposition, each polymeric nanowall has a width of ~170 nm and 1.4 μm in height (i.e., aspect ratio of ~8.2), as shown in Figure 2(a). On one sides of these polymeric walls, we deposited thin aluminum layers until the deposited metal film had a thickness of about 50 nm. Upon buckling, the average amplitude of resulting wrinkles, observed from the SEM image, was estimated to be approximately 1 μm. The observed lateral wrinkling patterns shown in Figure 2(b) are totally different from the conventional random buckles observed on flat surfaces, as shown in the supporting information Figure S1.

The SEM images of nanowalls with different wall spacings are shown in **Figure 3**. Aluminum was obliquely deposited at an angle of 30° with respect to the surface normal. When the space between nanowalls is small, as shown in Figure 3(a), the metal deposited does not cover the entire faces of selected sides of polymeric nanowalls. However, when the space is large enough, aluminum metal films could cover the entire faces of selected sides of polymeric nanowalls as well as some bottom parts of a substrate. It is interesting to note that the degree of buckling became higher when the metal film does not fully cover the bottoms of the nanowalls. When the metal film covered the entire selected sides of nanowalls, the stiff metal films deposited at the bottom portion of the nanowalls resist the mechanical deformation induced by the residual stress at the top portion of nanowalls which is similar to free standing bilayer film. The top-views of buckled patterns with different wall spacings are shown in Figures 3(d–f).

Polymeric nanowalls with different wall widths and heights were also investigated. The film thickness of Al metal deposited was kept constant (~50 nm). **Figure 4** shows the SEM images of Janus nanowalls after the aluminum film deposition. The average wavelength of buckled nanowalls with a wall width of 290 nm and a height of 1.5 μm was about 7.4 μm. The wavelengths for the nanowalls with 170 nm and 130 nm wall widths were found to be about 4.4 μm and 3.6 μm respectively. Note that the average wavelength decreases with the decrease in wall width. In addition, when the space between nanowalls is narrow, we sometimes observe that the nanowalls are collapsed and merged together, as shown in Figure 4(c).

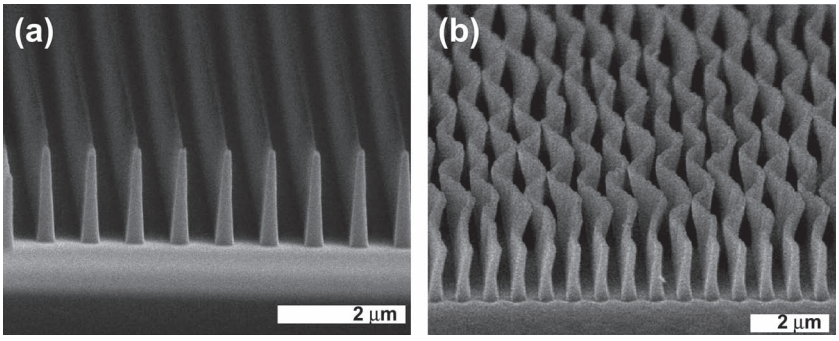

Figure 2. (a). A tilted SEM image of polymeric nanowalls before metal deposition. The average width of a nanowall is 170 nm and the wall height is 1.4 μm. (b) A tilted SEM image of Janus nanowalls containing thin aluminium films of 50 nm thickness on the left hand sides of the nanowalls.

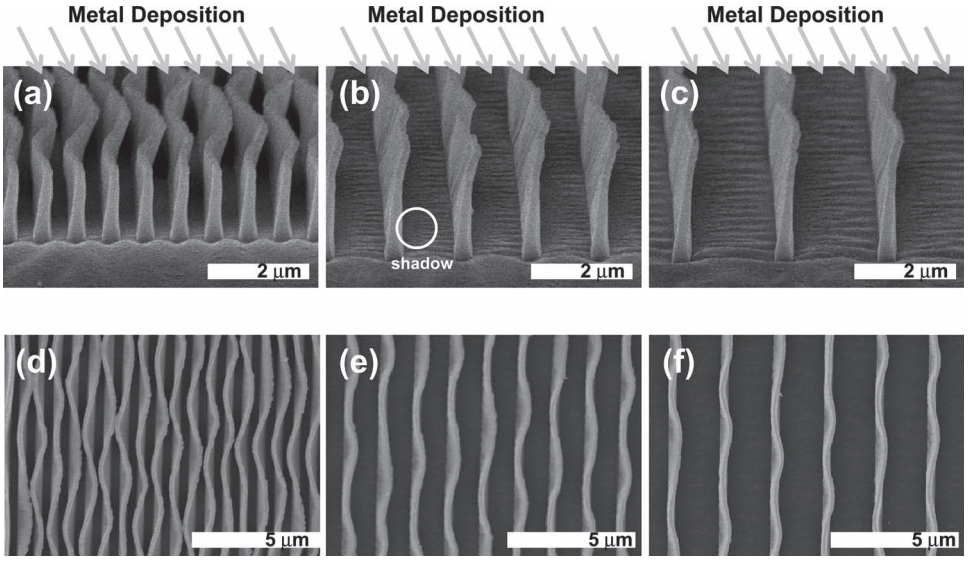

Figure 3. Tilted SEM images of Janus nanopillars with a height of 1.4 μm and an average wall width of 170 nm. The space between nanowalls is (a) 400 nm, (b) 900 nm, and (c) 1.6 μm, respectively. (d~f) Top-view SEM images of the Janus nanowalls shown in (a) to (c) with different spaces of (d) 400 nm, (e) 900 nm, and (f) 1.6 μm.

We now derive scaling relations between the amplitude and wavelength of wrinkles formed and the geometrical dimensions of nanowalls. **Figure 5** depicts a schematic illustration for the theoretical consideration of buckled Janus nanowalls. We assume that the faces of nanowalls exposed to metal deposition are fully covered by metal film. Once the induced strain on the polymer wall exceeds a critical value, buckling is spontaneously induced by the geometric confinement at the base where the wall is attached to the substrate. We sacrifice rigour for simplicity; our assumptions are justified by the good agreement of the predictions with experimental observations.

We assume that the magnitude of residual stress exerted on polymer walls is constant (denoted as σ). Let ν denote the Poisson's ratio of crosslinked polymer walls and E the Young's modulus.

We denote the vertical plane of initially flat nanowall as the xy-plane and the out-of-plane displacement by ζ(x,y) that occurs along the z-axis. The flat wall has length L, height h and width w. The energy functional that we need to extremize for obtaining the Euler-Lagrange equations is:[32]

$$U = U_{bend} + U_{strech} - C \tag{1}$$

The first term U_{bend} is the bending energy associated with the wrinkles occurring mainly along the horizontal (y) direction:[16]

$$U_{bend} = 0.5\,B \int dA \left(\frac{\partial \zeta}{\partial y^2}\right) \tag{2}$$

We have ignored the energy associated with the bending in the x-direction because bending predominantly occurs in the y-direction; $B = Ew^3/[12(1-\nu^2)]$ is the bending modulus of polymeric wall.[16]

The second term U_{strech} is associated with the stretch of a nanowall along the vertical and the horizontal directions by the expanding metal layer deposited on one selected side of a polymeric nanowall.[16]

$$U_{stretch} = 0.5 \int dA \frac{F_x}{L} \left(\frac{\partial \zeta}{\partial x}\right)^2 + 0.5 \int dA \frac{F_y}{L} \left(\frac{\partial \zeta}{\partial y}\right)^2 = 0.5 \int dA \sigma w \left(\frac{\partial \zeta}{\partial x}\right)^2 + 0.5 \int dA \sigma w \left(\frac{\partial \zeta}{\partial y}\right)^2 \tag{3}$$

We have assumed F(x) ~ σLw and F(y) ~ σhw where we have assumed the residual stress σ to be constant in both horizontal and vertical directions.

The third term in Equation (1) expresses the constraint. The net expansion in the horizontal direction is the balance between the expansion due to stretching and the contraction due to the Poisson effect.

Let δ(x)/L be the horizontal strain due to the Poisson effect.[16]

$$\delta(x)/L = \upsilon\sigma/E \tag{4}$$

It may be noted that since we have assumed σ ~ constant and isotropic, the horizontal increase in length due to the metal expansion is σ/E. Thus, the balance of the above effects could happen if $\nu = 1.0$. But no material is known to have the Poisson ratio of unity. So there is always a net expansion due to the stretching of the polymer wall by the expanding metal thin layer. From the analysis provided in the supporting information S2, we could obtain the analysis of the amplitude A and wave number q by $A^2q^2 = 8\sigma(1-\nu)/E$. Also, the wavelength of wrinkles is found to be $\lambda = 2(2\pi h)^{1/2}(B/\sigma w)^{1/4}$ where h is the height and w is the wall width. Upon substituting $B = Ew^3/12(1-\nu^2)$, one finds a scaling relationship: $\lambda \sim (hw)^{1/2}$. It follows from the above relationship that the amplitude A scales as $(hw)^{1/2}$. It is worthwhile to note that if the polymer part of the bilayer is considerably thicker than the metal film (ideally infinite), the

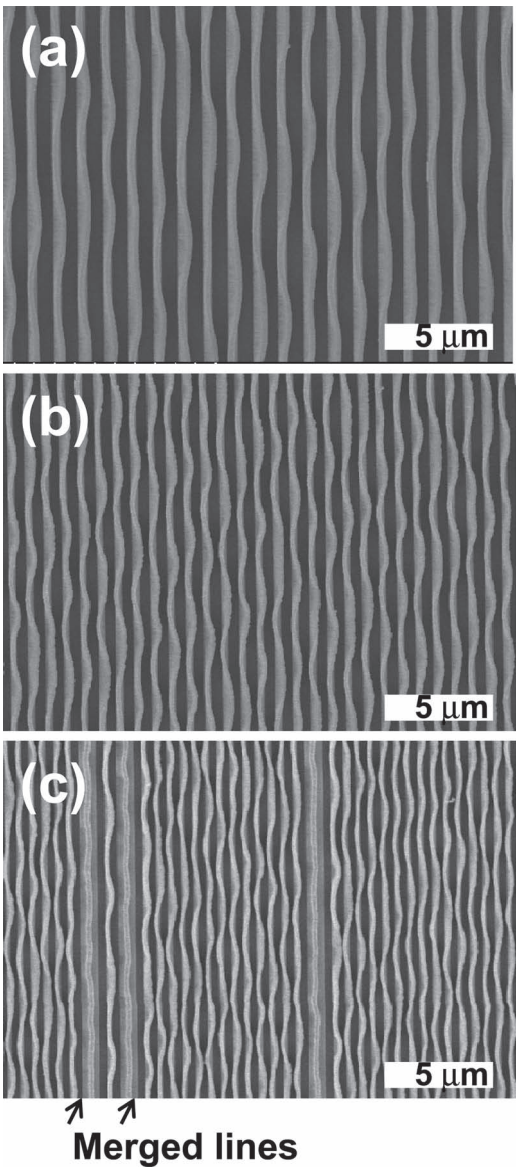

Figure 4. Plan-view SEM images of laterally buckled Janus nanowalls with wall widths of (a) 290 nm (height = 1.5 μm), (b) 170 nm (height = 1.4 μm), (c) 130 nm (height = 1.1 μm), respectively. The average wavelengths of buckled nanowalls are (a) 7.4 μm, (b) 4.4 μm, and (c) 3.6 μm, respectively.

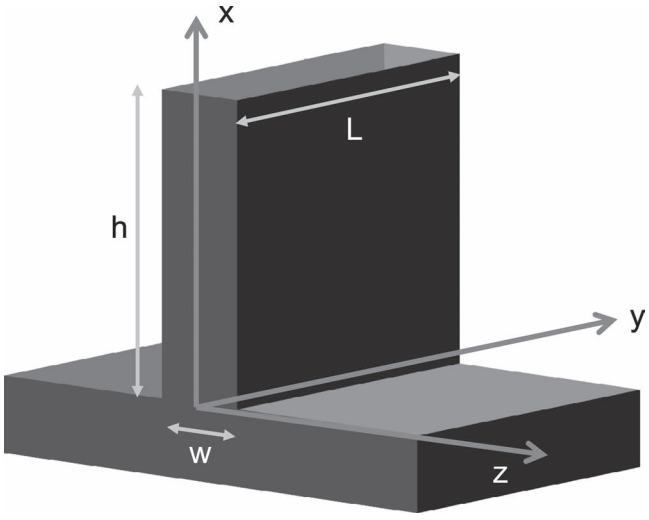

Figure 5. A schematic illustration for the theoretical consideration of buckled Janus nanowalls.

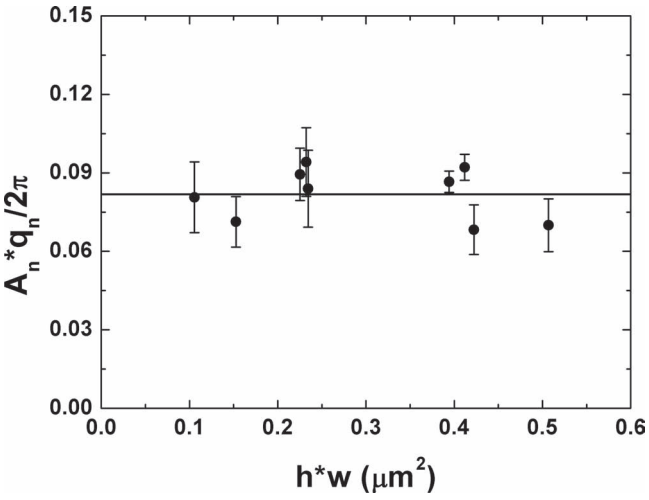

Figure 6. Plot of A*q (amplitude times the wavenumber of wrinkles) against the cross-sectional area of a nanowall (h*w). Solid dots represent the experimentally observed values; the solid line is obtained by linear regression. The product A*q should be independent of scaled width of nanowalls according to the scaling arguments. Experimental observation confirms the scaling prediction to a fair degree of accuracy.

wavelength of wrinkles on the surface is proportional to the thickness of a metal film.[27–29]

Figure 6 shows the plot of A*q against the cross-sectional area of a nanowall (h*w) - according to the scaling expression above, the product should be independent of cross-sectional area which is exactly what we observed in our experiments within the limits of experimental errors. The dots represent experimentally observed values while the solid line is obtained by the linear regression. It is noted that we could obtain the Young's modulus of a polymer substrate (E) from the values of the Poison ratio, the residual stress of Al[15] as well as the constant A*q value taken from Figure 6. The calculated modulus is approximately 16 MPa, which is relevant to the Young's modulus of the polymer (19.8 MPa) obtained from independent measurements.[31] A plot of A^2 against the cross-sectional area of a nanowall (h*w) is also shown in **Figure 7**. The dots represent the experimentally observed values while the solid line is obtained by the linear regression. The scaling prediction of the linear dependence of A^2 against h*w shows an excellent agreement with the experimental observations as well. Our scaling and experimental results indicate that the instability induced by the stress as well as the geometric confinement is of Cerda–Mahadevan type for the wrinkles in free standing films.[32]

Prior studies have reported various types of wrinkles caused by the heat expansion[27,28] based on different expansion coefficients between metals or oxide films and elastomers, by stretching or compressing the elastomeric substrates based on different Young's moduli between bilayers.[29] The wrinkling of bilayer surface induced by solvent evaporation has also been reported.[33] However, buckling in Janus nanowalls, as observed in our experiments, is induced by the residual stresses of metals deposited as well as geometric constraints. When the deposited metal film exerts compressive residual stress against polymeric nanowalls, the metal film stretches the polymer walls. On the other hand, when the metal film is under tensile stress, the metal film is stretched and eventually induces cracks of metal film at the interfaces between metal and polymeric layers during relaxation. **Figure 8** shows the difference in effects induced by two different metal films. We deposited Al and Au films of the same thickness (~50 nm) with a controlled rate of deposition of more than 100 Å/min to exclude the effect of thermal expansion of polymer nanowalls. Figure 8(a) shows a plan-view SEM image after Al deposition. The Janus nanowalls are buckled as we expected. However, when we deposited Au instead, there was no buckling of Janus nanowalls, as shown in the top-view SEM image of Figure 8(b). Instead of forming wrinkles on the substrate, several cracks of Au films (shown in circles) were observed at the bottom substrate. Figure 8(c) shows a tilted SEM image of buckled Janus nanowalls after Al deposition. As marked by a circle in the figure, there also exists a buckling on the flat polymer substrate which is induced by the same compressive residual stress of Al. Figure 8(d), however, shows that nanowalls deposited with gold thin layers on one selected side of the walls are instead bent toward the gold deposited side, which is in coincidence with the case with nanopillars in our previous work.[15]

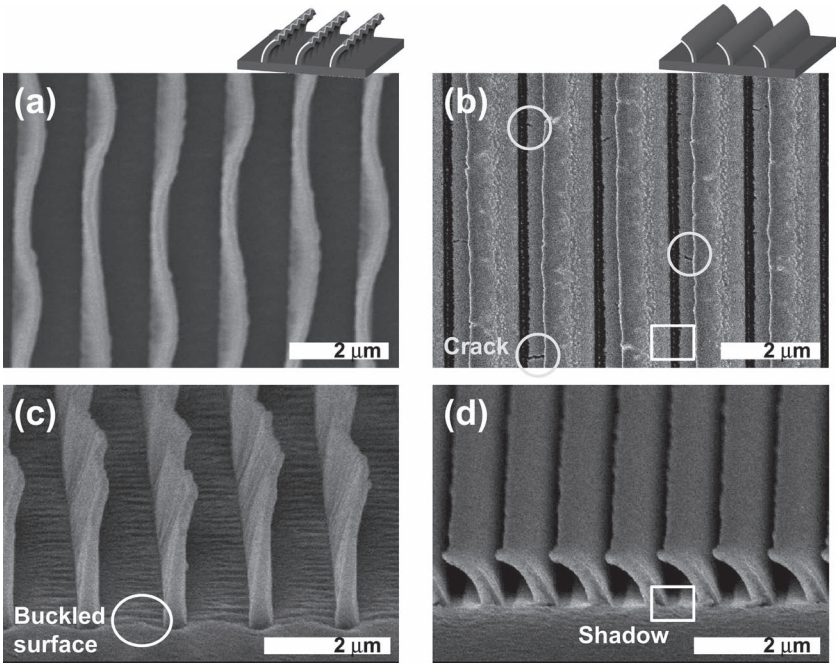

Figure 8. (a) A plan-view SEM image of Al-deposited Janus nanowalls. (b) A top-view SEM image of Au-deposited Janus nanowalls. The circles show that the gold films deposited on the polymer substrate form cracks because of their inherent residual tensile stress. The white open square shows a shadow in which metal is not deposited. (c) A tilted SEM image of Al-deposited Janus nanowalls. The white open circle also shows the buckling on a flat polymeric surface due to the residual compressive stress of Al thin film deposited. (d) A tilted SEM image of Au-deposited Janus nanowalls are bent toward the metal-deposited sides. The image also represents that there is no lateral buckling during the Au deposition.

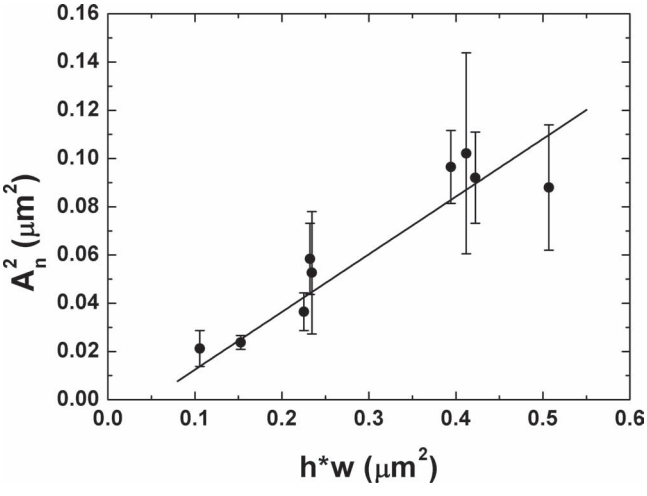

Figure 7. Plot of A^2 against the cross-sectional area of a nanowall (h*w); solid circles represent the experimentally observed values while the solid line is obtained by linear regression. The theoretical prediction of the linear dependence of A^2 on h*w shows an excellent agreement with the experimental observations.

3. Conclusions

In the present study, we report the fabrication of novel nanostructures–*Janus nanowalls*. Such a structure consists of bilayers with a metal thin layer deposited obliquely on one selected face of a polymeric wall standing vertically against a solid substrate. During the oblique metal deposition, the lateral buckling of Janus nanowalls was spontaneously induced in our experiments. We indicate that the vertical bilayer geometry is novel and the buckling features are entirely different from the horizontal bilayer cases described in previous studies.[23–25] The buckling of Janus nanowalls and the wrinkle formation after the aluminium deposition is caused by geometric confinements as well as the residual compressive stress of a deposited metal film exerted on polymeric nanowalls. We employed scaling arguments to investigate the main features of wrinkling patterns induced by the lateral buckling. Our scaling results for the wavelength and amplitude of wrinkles formed on nanowalls are in good agreement with the experimental observations,

suggesting that the instability in the current case is of Cerda–Mahadevan type.[32]

4. Experimental Section

Fabrication of Janus nanowalls: Silicon master molds were prepared by the photolithography followed by reactive ion etching. Those silicon masters were then treated with a fluorinated-SAM solution ((tridecafluoro-1,1,2,2-tetrahydrooctyl)-trichlorosilane: FOTCS, Gelest Corp.) diluted to 0.03 M with anhydrous heptane (Samchon Corp.) in inert argon environment. The treated master molds were annealed at 120 °C for 20 min. Onto the Si masters, we applied drops of soft PUA (301RM, Minuta Tech) prepolymers and a flexible PET film (~50 μm) was slightly pressed against the liquid drop to be used as a supporting backplane. Details on the synthesis and characterization of PUA prepolymers can be found elsewhere.[30,31] After crosslinking the photocurable PUA polymers, we detached the polymeric structure from the Si master. We then deposited metal films (Al) by the oblique metal deposition with a film thickness of 50 nm. We used a thermal evaporator for the metal deposition and placed the polymeric nanostructure on an inclined holder, as discussed in the previous reports.[14,15] The vacuum condition for the metal deposition was 10^{-6} torr. During the deposition, evaporated metal atoms were vertically guided down, but the inclined holder defined the oblique incidence angle, leading to the metal layers deposited only on one selected sides of the nanowalls.

Scanning electron microscopy (SEM): High-resolution SEM images of wrinkled nanopatterns were obtained using Hitachi-4800S. To avoid the charging effects, all the polymer patterns were sputter-coated with Pt in 5 nm thickness prior to measurements.

Supporting Information

Supporting Information is available from the Wiley Online Library or from the author.

Acknowledgements

H.Y. and A.G. contributed equally to this work. This work was supported by the National Creative Research Initiative Center for Intelligent Hybrids (No. 2010-0018290) through the National Research Foundation of Korea (NRF) grants, the World Class University (WCU) Programs (R31-10013), and the Brain Korea 21 Program funded by the Ministry of Education, Science and Technology (MEST). W.B.L. acknowledges the support from Basic Science Research Program through the National Research Foundation of Korea (NRF) funded by the Ministry of Education, Science and Technology (2010-0007886), the Human Resources Development of the Korea Institute of Energy Technology Evaluation and Planning (KETEP) grant funded by the Korea government Ministry of Knowledge Economy (No. 2010T100100913).

Received: March 17, 2012
Revised: April 10, 2012
Published online: May 18, 2012

[1] P. G. de Gennes, *Rev. Mod. Phys.* **1992**, *64*, 645–648.
[2] J. Du, R. K. O'Reilly, *Chem. Soc. Rev.* **2011**, *40*, 2402–2416.
[3] S. C. Glotzer, M. J. Solomon, *Nat. Mater.* **2007**, *6*, 557–562.
[4] Q. Chen, S. C. Bae, S. Granick, *Nature* **2011**, *469*, 381–384.
[5] Q. Chen, J. K. Whitmer, S. Jiang, S. C. Bae, E. Luijten, S. Granick, *Science* **2011**, *331*, 199–202.
[6] K.-H. Roh, D. C. Martin, J. Lahann, *Nat. Mater.* **2005**, *4*, 759–763.
[7] S. Jiang, Q. Chen, M. Tripathy, E. Luijten, K. S. Schweizer, S. Granick, *Adv. Mater.* **2010**, *22*, 1060–1071.
[8] A. Perro, S. Reculusa, S. Ravaine, E. Bourgeat-Lami, E. Duguet, *J. Mater. Chem.* **2005**, *15*, 3745–3760.
[9] A. Walther, A. H. E. Muller, *Soft Matter* **2008**, *4*, 663–668.
[10] T. Nisisako, T. Torii, T. Takahashi, Y. Takizawa, *Adv. Mater.* **2006**, *18*, 1152–1156.
[11] M. D. McConnell, M. J. Kraeutler, S. Yang, R. J. Composto, *Nano Lett.* **2010**, *10*, 603–609.
[12] A. Walther, K. Matussek, A. H. E. Müller, *ACS Nano* **2008**, *2*, 1167–1178.
[13] M. Yoshida, K.-H. Roh, J. Lahann, *Biomaterials* **2007**, *28*, 2446–2456.
[14] H. Yoon, H. E. Jeong, T.-i. Kim, T. J. Kang, D. Tahk, K. Char, K. Y. Suh, *Nano Today* **2009**, *4*, 385–392.
[15] H. Yoon, H. Woo, M. K. Choi, K. Y. Suh, K. Char, *Langmuir* **2010**, *26*, 9198–9201.
[16] L. D. Landau, E. M. Lifshitz, *Theory of Elasticity*, 3rd ed., Butterworth-Heinemann, Oxford, UK **1984**.
[17] J. M. Gere, S. P. Timoshenko, *Mechanics of Materials*, 4th ed., PWS publishing Company, Boston, USA **1997**.
[18] H. Liang, L. Mahadevan, *Proc. Natl, Acad. Sci. USA* **2011**, *108*, 5516–5521.
[19] J. Huang, B. Davidovitch, C. D. Santangelo, T. P. Russel, N. Menon, *Phy. Rev. Lett.* **2010**, *105*, 038302.
[20] T. Tallinen, J. Ojajärvi, J. A. Åström, J. Timonen, *Phy. Rev. Lett.* **2011**, *105*, 066102.
[21] Y. Klein, E. Efrati, E. Sharon, *Science* **2007**, *315*, 1116–1120.
[22] Y. Klein, S. Venkararamani, E. Sharon, *Phys. Rev. Lett.* **2011**, *106*, 118303.
[23] J. Kim, J. A. Hanna, M. Byun, C. D. Santangelo, R. C. Hayward, *Science* **2012**, *335*, 1201–1205.
[24] S. Yang, K. Khare, P.-C. Lin, *Adv. Funct. Mater.* **2010**, *20*, 2550–2564.
[25] S. J. DuPont Jr., R. S. Cates, P. G. Stroot, R. Toomey, *Soft Matter* **2010**, *6*, 3876–3882.
[26] M. K. Kang, R. Huang, *Int. J. Appl. Mech.* **2011**, *3*, 219–233.
[27] N. Bowden, S. Brittain, A. G. Evans, J. W. Hutchinson, G. M. Whitesides, *Nature* **1998**, *393*, 146–149.
[28] P. J. Yoo, K. Y. Suh, S. Y. Park, H. H. Lee, *Adv. Mater.* **2002**, *14*, 1383–1387.
[29] C. M. Stafford, C. Harrison, K. L. Beers, A. Karim, E. J. Amis, M. R. Van Landingham, H.-C. Kim, W. Volksen, R. D. Miller, E. E. Simonyi, *Nat. Mater.* **2004**, *3*, 545–550.
[30] S.-J. Choi, P. J. Yoo, S. J. Baek, T. W. Kim, H. H. Lee, *J. Am. Chem. Soc.* **2004**, *126*, 7744–7745.
[31] P. J. Yoo, S. Choi, J. H. Kim, D. Suh, S. J. Beak, T. W. Kim, H. H. Lee, *Chem. Mater.* **2004**, *16*, 5000.
[32] J. S. Sharp, R. A. L. Jones, *Adv. Mater.* **2002**, *14*, 799–802.
[33] E. Cerda, L. Mahadevan, *Phys. Rev. Lett.* **2003**, *90*, 074302.